

Characterization of maximally random jammed sphere packings: Voronoi correlation functions

Michael A. Klatt

*Department of Chemistry, Department of Physics,
Princeton University, Princeton, New Jersey 08544, USA and
Friedrich-Alexander-Universität Erlangen-Nürnberg (FAU),
Institut für Theoretische Physik, Staudtstraße 7, 91058 Erlangen, Germany*

Salvatore Torquato*

*Department of Chemistry, Department of Physics,
Princeton Institute for the Science and Technology of Materials,
and Program in Applied and Computational Mathematics,
Princeton University, Princeton, New Jersey 08544, USA*

(Dated: March 3, 2022)

We characterize the structure of maximally random jammed (MRJ) sphere packings by computing the Minkowski functionals (volume, surface area, and integrated mean curvature) of their associated Voronoi cells. The probability distribution functions of these functionals of Voronoi cells in MRJ sphere packings are qualitatively similar to those of an equilibrium hard-sphere liquid and partly even to the uncorrelated Poisson point process, implying that such local statistics are relatively structurally insensitive. This is not surprising because the Minkowski functionals of a single Voronoi cell incorporate only local information and are insensitive to global structural information. To improve upon this, we introduce descriptors that incorporate nonlocal information via the correlation functions of the Minkowski functionals of two cells at a given distance as well as certain cell-cell probability density functions. We evaluate these higher-order functions for our MRJ packings as well as equilibrium hard spheres and the Poisson point process. It is shown that these Minkowski correlation and density functions contain visibly more information than the corresponding standard pair-correlation functions. We find strong anticorrelations in the Voronoi volumes for the hyperuniform MRJ packings, consistent with previous findings for other pair correlations [A. Donev *et al.*, Phys. Rev. Lett. 95, 090604 (2005)], indicating that large-scale volume fluctuations are suppressed by accompanying large Voronoi cells with small cells, and vice versa. In contrast to the aforementioned local Voronoi statistics, the correlation functions of the Voronoi cells qualitatively distinguish the structure of MRJ sphere packings (prototypical glasses) from that of not only the Poisson point process but also the correlated equilibrium hard-sphere liquids. Moreover, while we did not find any perfect icosahedra (the locally densest possible structure in which a central sphere contacts 12 neighbors) in the MRJ packings, a preliminary Voronoi topology analysis indicates the presence of strongly distorted icosahedra.

I. INTRODUCTION

Packings of frictionless monodisperse hard spheres in three dimensions serve as a simple, yet effective tool for modeling the complex behavior of such diverse many-particle systems as crystals, colloids, liquids, glasses, heterogeneous materials, foams, and biological systems [1–10]. Among the rich multitude of states they are known to exhibit, considerable interest has been given towards sphere packings that are jammed (i.e., mechanically stable), including maximally dense packings, low-density crystals, and amorphous packings [11–20].

In order to characterize the properties of sphere packings, one may employ a geometric-structure approach in which configurations are considered independently of both their frequency of occurrence and the algorithm by which they are created [19]. For example, the simplest characteristic of a sphere packing is its packing fraction

ϕ , i.e., the fraction of space occupied by the spheres. Other useful characteristics of the structure include its pair-correlation function [14, 21–28], the pore-size distribution [4, 29], and structure factor [3, 24, 30–32].

It is also valuable to quantify the degree of ordering in a packing, especially those that are jammed (defined more precisely below). To this end, a variety of scalar order metrics ψ have been suggested [19, 33] in which $\psi = 0$ is defined as the most disordered state (i.e. the Poisson point process) and $\psi = 1$ is the most ordered state. Using the geometric-structure approach, one may therefore construct an “order map” in the ϕ – ψ plane [19], where the jammed packings form a subset in this map. The boundaries of the jammed region are optimal in some sense, including, for example, the densest packings (the face-centered-cubic crystal and its stacking variants with $\phi_{\max} = \pi/\sqrt{18} \approx 0.74$ [13]) and the least dense jammed packings (conjectured to be the “tunneled crystals” with $\phi_{\min} = 2\phi_{\max}/3$ [16]).

Among the set of all isotropic and statistically homogeneous jammed sphere packings, the maximally random

* Electronic mail: torquato@electron.princeton.edu

jammed (MRJ) state is that which minimizes some order metric ψ . This definition makes mathematically precise the familiar notion of random closed packing (RCP) in that it can be unambiguously identified for a particular choice of order metric. A variety of sensible, positively correlated order metrics produce an MRJ state with the same packing fraction 0.64 [34, 35], which agrees roughly with the commonly suggested packing fraction of RCP in three dimensions [19]. However, we stress that density alone is not sufficient to characterize a packing; in fact, packings with a large range of ψ may be observed at this packing fraction [27, 34].

In order to study the MRJ state, a precise definition of jamming is needed. Therefore, rigorous hierarchical jamming categories have been defined [36, 37]: A packing is *locally jammed* if no particle can move while the positions of the other particles are fixed; it is *collectively jammed* if no subset of particles can move without deforming the system boundary; and if also a deformation of the system boundary is not possible without increasing its volume, the packing is *strictly jammed*, i.e., it is stable against both uniform compression and shear deformations [38]. Strictly jammed MRJ sphere packings often contain a small fraction of rattlers (unjammed particles), but the remainder of the packing, i.e., the mechanically rigid backbone, is strictly jammed [39].

Determining the contact network of a packing is a subtle problem requiring high numerical fidelity. The Torquato-Jiao (TJ) sphere packing algorithm [25] meets this challenge by efficiently producing highly disordered, strictly jammed packings with unsurpassed numerical fidelity as well as ordered packings [25, 40]. The algorithm achieves this by solving a sequence of linear programs which iteratively densify a collection of spheres in a deformable periodic cell subject to locally linearized nonoverlap constraints. The resulting packings are, by definition, strictly jammed and they are with high probability exactly isostatic (meaning that they possess the minimum number of contacts required for jamming) [39, 41]. The TJ packing protocol is intrinsically capable of producing MRJ states with very high fidelity [25, 39]. The MRJ state can be regarded as a prototypical glass because it is maximally disordered (according to a variety of order metrics) while having infinite elastic moduli [19]. Atkinson *et al.* [39] recently carried out a detailed characterization of the rattler population in these MRJ sphere packings. They found a rattler fraction of 1.5% (substantially lower than other packing protocols, such as the well-known Lubachevsky-Stillinger packing algorithm [42]) and that the rattlers were highly spatially correlated, implying that they have a significant influence on the structure of the packing [29]. Moreover, as in previous studies [41], it was shown [39] that the backbone of the MRJ state is isostatic. We include rattlers in our analysis unless stated otherwise.

MRJ packings have been characterized using a variety of statistical descriptors, including the radial pair-correlation function $g_2(r)$ ($\rho^2 g_2$ is the probability den-

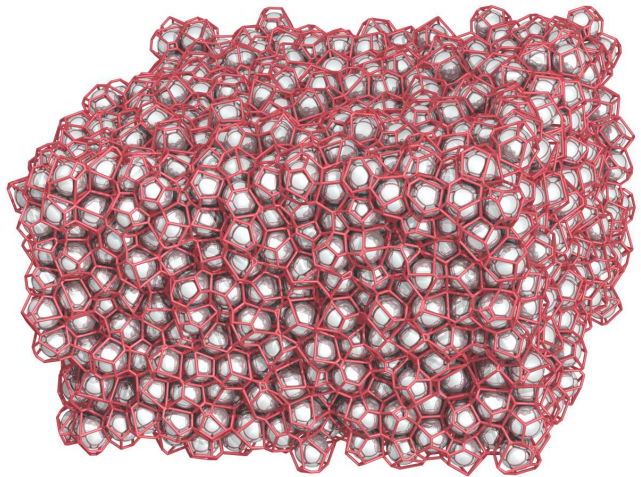


FIG. 1. (Color online) Maximally random jammed (MRJ) sphere packing and its Voronoi diagram. Among all jammed sphere packings (roughly speaking, the mechanically stable packings), the MRJ state is the most disordered one.

sity for finding two sphere centers separated by a radial distance r , where ρ is the number density, i.e., the number of particles per unit volume) [25], the bond-orientational order metric Q_6 and the translational order metric T^* [34, 39], the cumulative pore-size distribution $F(\delta)$ [29], and the statistics of rattlers [39]. In addition, MRJ sphere packings exhibit disordered hyperuniformity [29], meaning that they are locally disordered, but possess a hidden order on large length scales such that infinite-wavelength density fluctuations of MRJ packings vanish, i.e., the structure factor vanishes at the origin: $\lim_{\mathbf{k} \rightarrow 0} S(\mathbf{k}) = 0$ [43, 44]. Disordered hyperuniformity can be seen as an “inverted critical phenomenon” with a direct correlation function $c(r)$ that is long ranged [43, 45].

In this paper, we characterize the MRJ sphere packings generated in Ref. [39] using Voronoi statistics, including certain types of correlation functions. We compare these computations to corresponding calculations for both a Poisson distribution of points and equilibrium hard-sphere liquids. In the second paper of this series, we will investigate density fluctuations, the pore-size distribution, and two-point probability functions of MRJ packings.

Many studies for disordered sphere packings have been devoted to computing the volume distribution of the Voronoi cells [e.g., 15, 17, 20, 46–52]; see Fig. 1 for a MRJ sphere packing and its Voronoi diagram [53]. However, such statistics are incomplete in that they only quantify local structural information. For example, with appropriately rescaled variables, we will show that the distributions of the Voronoi volumes, surface areas, and integrated mean curvatures for the MRJ sphere packings are qualitatively similar to the distributions for an equilibrium hard-sphere liquid and partly even for the spatially uncorrelated Poisson point process.

TABLE I. Mean $\langle W_\mu \rangle$, standard deviation σ_{W_μ} , and correlation coefficients $\rho_{\mu,\nu}$ of the Minkowski functionals W_μ of single Voronoi cells in the Poisson point process, in a system of hard spheres in equilibrium at a packing fraction $\phi = 0.48$, and in the MRJ state. The unit of length is $\lambda = 1/\rho^{1/3}$, i.e., the number density ρ is set to unity.

		$\langle W_\mu \rangle$	σ_{W_μ}	$\rho_{\mu,1}$	$\rho_{\mu,2}$
Poisson					
Volume	W_0	1.0005(3)	0.4230(2)	0.98161(3)	0.94486(8)
Surface area	W_1	5.823(1)	1.4798(7)		0.98701(2)
Integ. mean curv.	W_2	9.1623(8)	1.0941(5)		
Equilibrium					
Volume	W_0	1.00000(7)	0.07434(5)	0.97700(5)	0.9282(2)
Surface area	W_1	5.4488(3)	0.2681(2)		0.98136(5)
Integ. mean curv.	W_2	8.6477(2)	0.2163(2)		
MRJ					
Volume	W_0	1.00000(3)	0.04335(2)	0.96976(4)	0.9035(1)
Surface area	W_1	5.4043(1)	0.1695(8)		0.97248(5)
Integ. mean curv.	W_2	8.5894(1)	0.1470(7)		

To quantify nonlocal structural information, we formulate and compute correlation functions of the volume of Voronoi cells at a given distance and cell-cell probability density functions of finding a given sized Voronoi cell at a given distance of a sphere with another sized Voronoi cell. Because the volume is only one of a large class of versatile shape measures, namely, the Minkowski functionals [54–57], we devise and compute the correlation functions of all of the Minkowski functionals [58]. Besides characterizing MRJ packings in this way, we also carry out analogous calculations for the Poisson point process and the equilibrium hard-sphere liquid for purposes of comparison. We show that these Minkowski correlation functions contain visibly more information than the corresponding standard pair-correlation functions, even in the case of the Poisson point process.

In Sec. II, we analyze the distributions of the Minkowski functionals of the single Voronoi cells for the Poisson point process, equilibrium hard-sphere liquid configurations, and MRJ packings. In Sec. III, we define the aforementioned two different types of correlation functions. In Sec. IV, we determine the volume-volume correlation function numerically for the three-dimensional Poisson point process, equilibrium hard-sphere systems, and the MRJ state; we also calculate the correlation functions for the surface area, and the integrated mean curvature. For a further investigation of the nonlocal structure features, we calculate in Sec. V the cell-cell probability density functions mentioned above. In Sec. VI, we make concluding remarks.

II. MINKOWSKI FUNCTIONAL DISTRIBUTIONS OF A SINGLE VORONOI CELL

While there are many detailed studies of the volume distribution in disordered sphere packings [e.g., 15, 17, 20, 46–52], here we analyze in a logarithmic plot the volume distributions of true MRJ packings as describe above and extend the analysis to all three (non-

trivial) Minkowski functionals: the volume, the surface area, and the integrated mean curvature. They are robust and versatile shape descriptors which are widely used in statistical physics [55–57, 59] and in pattern analysis [60–62]. We use VORO++ [63, 64] to construct the Voronoi diagram of Poisson point patterns (about 1000 patterns, each with 2000 points), equilibrium hard-sphere packings [3, 4] at a packing fraction $\phi = 0.48$, which is slightly below the freezing transition (100 packings, each with 10000 spheres), and MRJ sphere packings produced by the TJ algorithm [25, 39] (about 1000 packings, each with 2000 spheres). The program KARAMBOLA [65, 66] then computes the Minkowski functionals of each cell.

We first determine the distributions of the three Minkowski functionals (W_0 , volume; W_1 , surface area; and W_2 , integrated mean curvature) of the single Voronoi cells. Table I provides the mean, the standard deviation, and the correlation coefficients $\rho_{\mu,\nu} = \frac{\langle W_\mu W_\nu \rangle - \langle W_\mu \rangle \langle W_\nu \rangle}{\sigma_{W_\mu} \sigma_{W_\nu}}$ of the three different Minkowski functionals. As a unit of length, we use $\lambda = 1/\rho^{1/3}$ with ρ the number density, i.e., we compare the Poisson point process, the equilibrium hard-sphere liquid, and the MRJ state at the same number density $\rho = 1$ (the unit volume contains one particle on average) [67].

Because the number density is set to unity, the mean cell volume is also one. The average surface area and integrated mean curvature of a Voronoi cell in the MRJ state or in the equilibrium ensemble are slightly larger than those of a Poisson Voronoi cell because the latter is less regular, i.e., more aspherical. The Voronoi volume fluctuations and the standard deviations of the other Minkowski functionals are much stronger in the irregular Poisson point process than in the hard-sphere packings, where the MRJ state has significantly smaller Voronoi volume fluctuations than the equilibrium hard-sphere liquid. The Minkowski functionals of a single Voronoi cell, e.g., its volume and its surface area, are strongly correlated, i.e., the correlation coefficients $\rho_{\mu,\nu}$ are at least 0.9. The numerical estimates for the Poisson Voronoi tes-

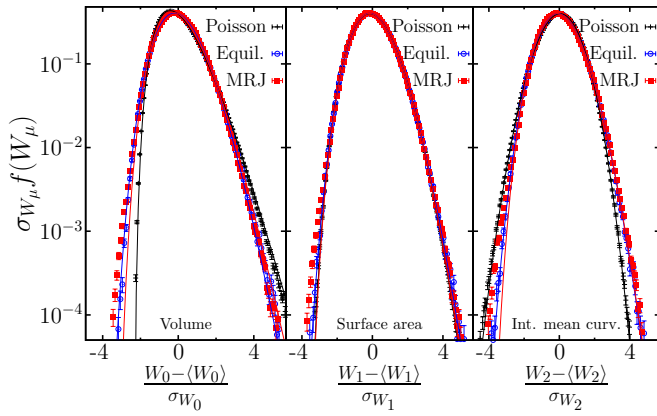


FIG. 2. (Color online) Distributions of the single Minkowski functionals W_μ of a three-dimensional Voronoi cell in a Poisson point process, an equilibrium hard-sphere system at a packing fraction $\phi = 0.48$, and a MRJ sphere packing: $\mu = 0$ volume (left), $\mu = 1$ surface area (center), and $\mu = 2$ integrated mean curvature (right). The distributions are rescaled—like in Ref. [47]—by their mean $\langle W_\mu \rangle$ and their standard deviation σ_{W_μ} (see Table I). The lines in the plot of the volume distributions are γ distributions; generalized γ distributions are fitted to the distributions of the surface area and the integrated mean curvature.

sellation are in agreement with the analytic values and numerical estimates in Ref. [68] and references therein.

The high fidelity of the MRJ sphere packings produced by the TJ algorithm allows one to study the relation between the number of contacts of a sphere and the Minkowski functionals of its Voronoi cell. As expected, small cells have a higher number of contacts on average because a high local packing fraction [69] implies that there are many close neighbors. In units of λ , the mean Voronoi volume of a rattler, i.e., an unjammed particle, is 1.04 and that of a particle with 11 contacts is 0.88. The mean surface area of the Voronoi cells of rattlers and of backbone spheres with up to 11 contacts varies from 5.50 to 4.92, respectively, and the average integrated mean curvature varies from 8.65 to 8.17, respectively. However, because of the small difference between near contacts and true contacts, the distributions of the Minkowski functionals for rattlers are only slightly shifted compared to the distributions of a typical cell. There are, for example, very small cells containing rattlers, which is consistent with previous findings [39].

Starr *et al.* [47] and, similarly, Aste *et al.* [15] showed that by shifting the volume distribution by its mean and rescaling with its standard deviation, the volume distributions of many different sphere packings collapse. Figure 2 shows the rescaled distributions of the Minkowski functionals for the Poisson point process, the equilibrium hard-sphere liquid, and the MRJ packing. As expected, the volume distributions of the equilibrium hard-sphere packings and the MRJ packings are qualitatively very similar, while the distribution of the Poisson point process deviates. The same is true for the distribution of the

mean curvatures. The distributions of the surface area for both the MRJ and the equilibrium hard-sphere packings are not only qualitatively similar to each other but also to the uncorrelated Poisson point process. So, besides the quantitative difference in the mean and the standard deviations of the Minkowski functionals, the distributions of the Minkowski functionals of single Voronoi volumes are qualitatively similar for the equilibrium hard-sphere liquid and the MRJ state as well as even partially for the Poisson point process. The distribution of the Minkowski functionals of a single cell only incorporates local information and is rather insensitive to global structural features such as hyperuniformity of the MRJ state [29, 45].

Figure 3 shows the joint probability distribution of the volume and the surface area of a single Voronoi cell in a Poisson point process, an equilibrium hard-sphere liquid, and a MRJ sphere packing. The joint probability distributions for the equilibrium hard-sphere liquid and the MRJ state are also relatively similar.

Both for the Poisson point process [70] and for many different numerical and experimental sphere packings [15], the volume distribution follows well a γ distribution [71]. We also find, for the volume distributions for the Poisson point process and the equilibrium hard-sphere liquid, an excellent agreement with γ distributions [72]. However, for the MRJ sphere packings there is a slight but statistically significant deviation for very small cells for which the frequency of occurrence is too high. The surface area and the integrated mean curvature distributions are well approximated by generalized γ distributions [73], which was already found for the Poisson point process by Refs. [51, 74]. However, the distribu-

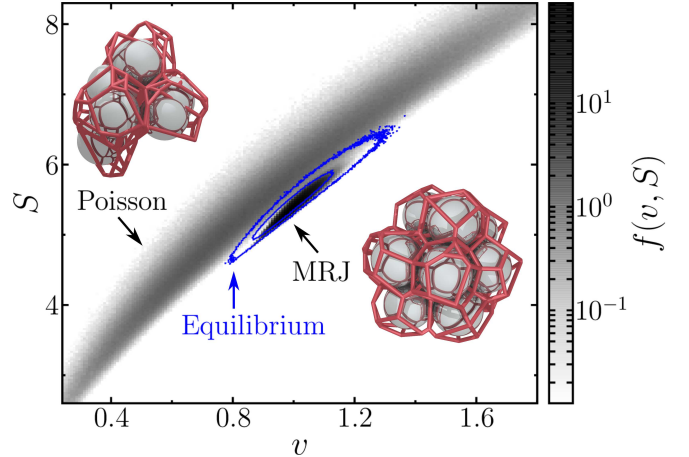


FIG. 3. (Color online) Joint distribution of volume v and surface area S of a single three-dimensional Voronoi cell in a log-logarithmic scale for a Poisson point process and a MRJ sphere packing; the joint distribution for the equilibrium hard-sphere liquid is represented by the blue contour plot. The unit of length is $\lambda = 1/\rho^{1/3}$, where ρ is the number density. Samples of a MRJ sphere packing and an overlapping sphere packing, where the sphere centers follow a Poisson point process, are depicted together with their Voronoi diagrams.

tions for the MRJ sphere packings deviate slightly but statistically significantly from a generalized γ distribution for cells with small surface area or small integrated mean curvature, respectively [75].

III. CORRELATION FUNCTIONS AND PROBABILITY DENSITY FUNCTIONS OF MINKOWSKI FUNCTIONALS

In order to quantify the global structure of the Voronoi diagram, correlation functions of the Minkowski functionals of cells at a distance r and cell-cell probability density functions are introduced and defined here.

A. Correlation Functions of Minkowski Functionals

We define the volume-volume correlation function $C_{00}(\mathbf{r}_1, \mathbf{r}_2)$ of the Voronoi cells of an arbitrary point process as the correlation between the volume of two Voronoi cells given that the corresponding centers are at the positions \mathbf{r}_1 and \mathbf{r}_2 :

$$C_{00}(\mathbf{r}_1, \mathbf{r}_2) := \frac{\langle v(\mathbf{r}_1)v(\mathbf{r}_2) \rangle - \langle v(\mathbf{r}_1) \rangle \langle v(\mathbf{r}_2) \rangle}{\sigma_{v(\mathbf{r}_1|\mathbf{r}_2)}\sigma_{v(\mathbf{r}_2|\mathbf{r}_1)}} \quad (1)$$

where $\langle \cdot \rangle$ denotes the ensemble average given two points at \mathbf{r}_1 and \mathbf{r}_2 ; and $\sigma_{v(\mathbf{r}_i|\mathbf{r}_j)}$ is the standard deviation of the volume v of the Voronoi cell at \mathbf{r}_i given that there is another point at \mathbf{r}_j . Note that because of this condition, both the mean and the standard deviation of a single Voronoi volume are functions of the positions \mathbf{r}_1 and \mathbf{r}_2 : e.g., knowing that there is a point in close proximity, very large volumes are less likely and the mean volume decreases. For a statistically homogeneous and isotropic point process, the volume-volume correlation is simply a radial function, which we denote by $C_{00}(r)$, where $r = \|\mathbf{r}_2 - \mathbf{r}_1\|$. The correlation function $C_{00}(r) \in [-1; 1]$ measures the correlations, both positive and negative (anticorrelations), between Voronoi volumes of cells given that their centers are at a distance r .

The Voronoi tessellation assigns to each point a volume of its corresponding Voronoi cell. This is a special case of a marked point process where the constructed mark assigned to each point is determined by the positions of the points in the neighborhood. In this sense, the volume-volume correlation function can be seen as a special type of a marked correlation function [56, 68, 76].

The volume-volume correlation function does not, in general, converge to perfect correlation for vanishing radial distance $\lim_{r \rightarrow 0} C_{00}(r) < 1$ because for all $r > 0$ the correlation function $C_{00}(r)$ provides the correlation of the Voronoi volumes of two different cells with volumes $v(0)$ and $v(r)$. Because the cell is perfectly correlated with itself, i.e., $C_{00}(0) = 1$, the correlation function $C_{00}(r)$ is discontinuous at the origin. If there is no long-range order, the correlation function tends to zero for infinite radial distance $\lim_{r \rightarrow \infty} C_{00}(r) = 0$.

The correlation functions of the other Minkowski functionals are defined analogously to Eq. (1), replacing volume ($\mu = 0$) by surface area ($\mu = 1$) or integrated mean curvature ($\mu = 2$):

$$C_{\mu\mu}(\mathbf{r}_1, \mathbf{r}_2) := \frac{\langle W_\mu(\mathbf{r}_1)W_\mu(\mathbf{r}_2) \rangle - \langle W_\mu(\mathbf{r}_1) \rangle \langle W_\mu(\mathbf{r}_2) \rangle}{\sigma_{W_\mu(\mathbf{r}_1|\mathbf{r}_2)}\sigma_{W_\mu(\mathbf{r}_2|\mathbf{r}_1)}} \quad (2)$$

with $\sigma_{W_\mu(\mathbf{r}_i|\mathbf{r}_j)}$ the standard deviation of the Minkowski functional W_μ of the Voronoi cell at \mathbf{r}_i given that there is another point at \mathbf{r}_j . For a statistically homogeneous and isotropic point process, the correlation function of the Minkowski functionals is again a radial function, which we denote by $C_{\mu\mu}(r)$. In general, $C_{\mu\mu}(r)$ will be discontinuous for $r \rightarrow 0$, as noted above for the volume-volume correlation function.

In the Appendix, we calculate the volume-volume correlation function analytically for the one-dimensional Poisson point process. In Sec. IV, we determine the correlation functions for the three-dimensional Poisson point process, the equilibrium hard-sphere liquid, and MRJ sphere packings.

A different type of correlation function, a pointwise Voronoi correlation function, assigns to arbitrary points the volumes of the Voronoi cells in which they lie [52]. Correlations between Voronoi volumes have also already been studied by finding a nonlinear scaling in the aggregate Voronoi volume fluctuations as a function of the sample size [49].

B. Cell-Cell Probability Density Functions of the Voronoi Volume

The volume-volume correlation function $C_{00}(\mathbf{r}_2, \mathbf{r}_1)$ is defined conditionally on the fact that the centers of the two cells are at \mathbf{r}_1 and \mathbf{r}_2 . The full two-point information about the Voronoi volumes is given by the cell-cell probability density function $p(\mathbf{r}_2, v, \mathbf{r}_1, v^*)$ of finding two points in the point process at two arbitrary positions \mathbf{r}_2 and \mathbf{r}_1 with associated Voronoi volumes v and v^* , respectively. It quantifies, for example, how likely it is to find near a point with a small Voronoi cell another point with either a large or another small Voronoi cell. Integrating over the volumes yields the standard pair-correlation function,

$$g_2(\mathbf{r}_2, \mathbf{r}_1) = \iint dv dv^* \frac{p(\mathbf{r}_2, v, \mathbf{r}_1, v^*)}{\rho(\mathbf{r}_2)\rho(\mathbf{r}_1)}. \quad (3)$$

This relation clearly indicates that the Minkowski probability density function $p(\mathbf{r}_2, v, \mathbf{r}_1, v^*)$ contains more information than $g_2(\mathbf{r}_2, \mathbf{r}_1)$. Moreover, the volume-volume correlation function $C_{00}(\mathbf{r}_2, \mathbf{r}_1)$ from Sec. III A follows from calculating the moments $\langle vv^* \rangle$, $\langle v \rangle$, and $\langle v^* \rangle$ of $\frac{p(\mathbf{r}_2, v, \mathbf{r}_1, v^*)}{\rho(\mathbf{r}_2)\rho(\mathbf{r}_1)g_2(\mathbf{r}_2, \mathbf{r}_1)}$ and the corresponding standard deviations σ_v and σ_{v^*} .

For a statistically homogeneous and isotropic point process, the cell-cell probability density function is a radial function, i.e., it only depends on the radial distance $r = |\mathbf{r}_2 - \mathbf{r}_1|$: $p(r, v, v^*)$ is the probability density of finding two points with Voronoi volumes v and v^* at a radial distance r . If there is no long-range order, the cell-cell probability density function $p(r, v, v^*)$ converges for large radii $r \rightarrow \infty$ to $\rho^2 f(v)f(v^*)$, with ρ the number density and $f(v)$ the distribution of the Voronoi volume v of a single cell (see Sec. II).

For a better visualization and comparison of different volumes, we divide the cell-cell probability density function by its long-range value; the cell-cell pair-correlation function is defined as

$$g_{vv}(\mathbf{r}_2, v, \mathbf{r}_1, v^*) := \frac{p(\mathbf{r}_2, v, \mathbf{r}_1, v^*)}{\rho(\mathbf{r}_2)f(v)\rho(\mathbf{r}_1)f(v^*)} \quad (4)$$

and, for a homogeneous and isotropic system,

$$g_{vv}(r, v, v^*) := \frac{p(r, v, v^*)}{\rho^2 f(v)f(v^*)}. \quad (5)$$

If $g_{vv}(r, v, v^*) > 1$, it is more likely to find a pair of Voronoi cells with volumes v and v^* at a distance r than to find them at a large distance, i.e., uncorrelated. If $g_{vv}(r, v, v^*) < 1$, the occurrence of a point in the point process with a Voronoi volume v at a distance r of another Voronoi center with a Voronoi volume v^* is suppressed. Analogous cell-cell pair-correlation functions can be defined for the other Minkowski functionals.

We analytically calculate the cell-cell probability density function for the one-dimensional Poisson point process in the Appendix. In Sec. V, we determine the cell-cell pair correlation function for the three-dimensional Poisson point process, the equilibrium hard-sphere liquid, and MRJ sphere packings.

IV. CORRELATION FUNCTIONS OF MINKOWSKI FUNCTIONALS

In order to sample the correlation functions of the Minkowski functionals, the distances of all pairs of particles [77] are computed and assigned to a bin. For each radial distance, i.e., for each bin, the correlation coefficient of the Minkowski functionals of the two Voronoi cells is determined.

Figures 4–6 compare the correlation functions of the Minkowski functionals for the Poisson point process, equilibrium hard-sphere liquids, and MRJ sphere packings. It is seen that these Minkowski correlation functions contain visibly more information than the corresponding standard pair-correlation functions, even in the case of the Poisson point process.

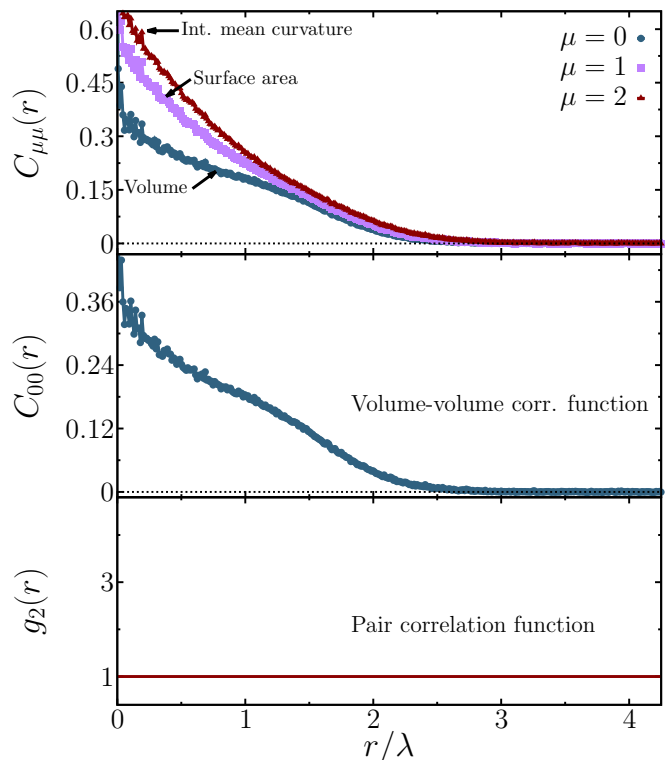


FIG. 4. (Color online) Correlation functions for a three-dimensional *Poisson point process*: pair-correlation function $g_2(r)$ (bottom); volume-volume correlation function $C_{00}(r)$ (center), which is the correlation function of the volumes of two Voronoi cells given that their centers are at a distance r ; the mark correlation functions of the three different Minkowski functionals (top): $\mu = 0$ volume, $\mu = 1$ surface area, and $\mu = 2$ integrated mean curvature. The radial distance r is normalized by $\lambda = 1/\rho^{1/3}$, where ρ is the number density.

A. Poisson Point Process

It is evident that in the infinite-system limit, the pair-correlation function $g_2(r)$ is a constant (unity) for the Poisson point process, i.e., the points are completely uncorrelated. Because a Voronoi cell is determined by the neighbors of its center, the volume will obviously be correlated; see Fig. 4. There are large Voronoi volume fluctuations for the Poisson point process. Very large cells lead to a strong correlation of the Voronoi volumes even for distances up to four times the mean nearest-neighbor distance. This is to be contrasted with the standard pair-correlation function $g_2(r)$, which is trivially unity for all radial distances.

Figure 4 compares the correlation functions $C_{\mu\mu}(r)$ for all Minkowski functionals $\mu = 0, 1, 2$. All functionals have approximately the same correlation length. For $r \rightarrow 0$, the surface areas are more strongly correlated than the volumes because at small radial distances, the cells will most likely share a face. In the Appendix, we calculate $C_{00}(r)$ analytically for the one-dimensional Poisson point

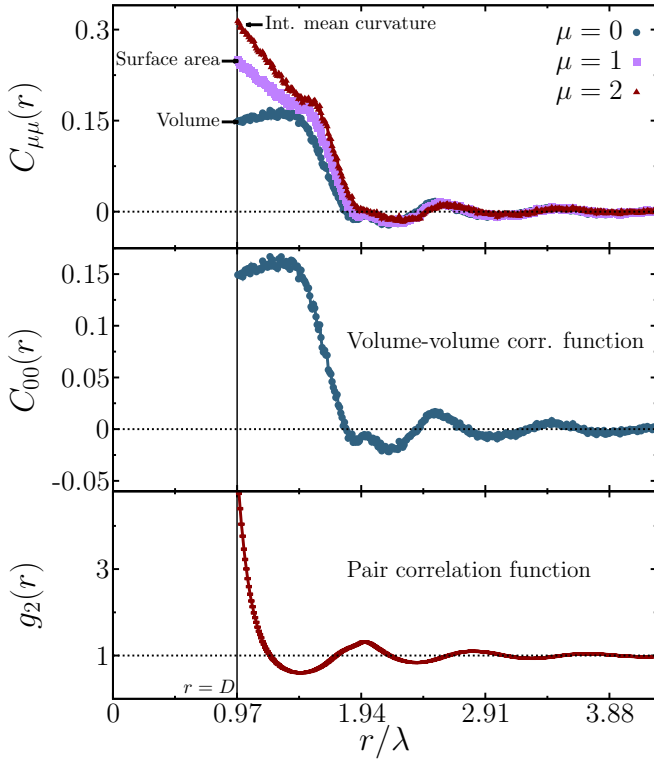


FIG. 5. (Color online) Correlation functions for *equilibrium hard spheres* with diameter D at a packing fraction $\phi = 0.48$; for details, see Fig. 4.

process.

B. Equilibrium Hard-Sphere Liquid

Figure 5 shows the pair-correlation function and the correlation functions of the Minkowski functionals for equilibrium hard-sphere liquid configurations at a packing fraction $\phi = 0.48$. Because the hard spheres are impenetrable, the correlation functions of the Minkowski functionals are only defined for radial distances larger or equal to the diameter D of a sphere; in this case, $D \approx 0.97\lambda$.

There is a strong correlation of the Voronoi volumes of spheres that are in near contact because the Voronoi neighbors are correlated by construction of the Voronoi diagram. However, the maximum correlation is reached for noncontacting spheres at $r \approx 1.3\lambda$; a large cell has many neighbors and a Voronoi neighbor with a sphere not in contact will be, on average, larger than another neighbor cell with a contacting sphere.

Between 1.8λ and 2.4λ , there is a double peak of anticorrelation and, for larger radial distances, there is an oscillating anticorrelation and correlation similar to the pair correlation function g_2 , but nearly inverted. The correlation length of the Voronoi volumes in the hard-sphere liquid is larger than in the uncorrelated Poisson point process, where the correlation was only due to the

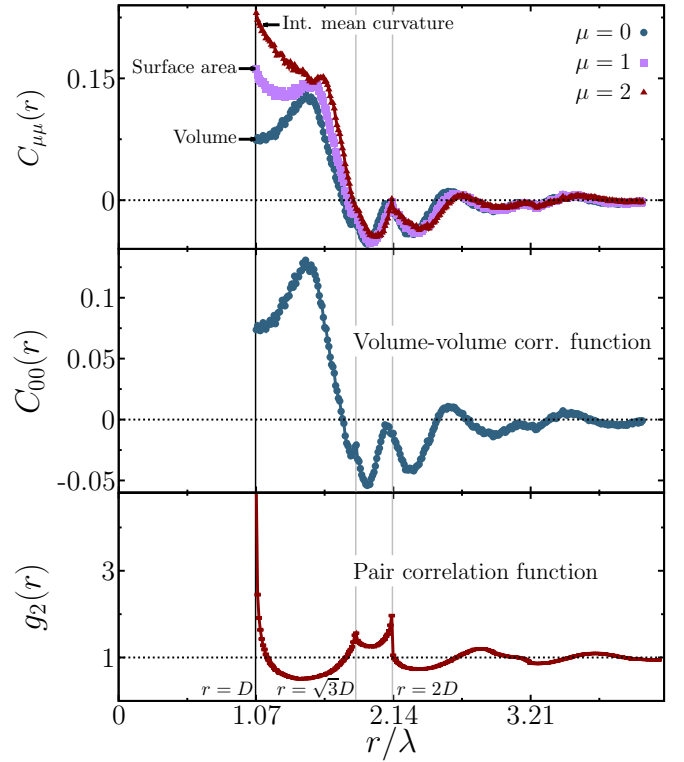


FIG. 6. (Color online) Correlation functions for *MRJ sphere packings* of spheres with diameter D ; the average packing fraction is $\phi \approx 0.64$. For details, see Fig. 4. The pair-correlation function $g_2(r)$ is in agreement with previous results for MRJ sphere packings [39].

large Voronoi volume fluctuations.

At the top of Fig. 5, the correlation functions of the other Minkowski functionals are compared. Similar to the Poisson case, the integrated mean curvature is more strongly correlated at contact $r = D$ than the surface area which, in turn, is more strongly correlated than the volume. There is no double anticorrelation peak in the integrated mean curvature. For large radii, the correlation functions are shifted against each other despite the strong correlation of the different functionals for a single Voronoi cell. The surface area and the integrated mean curvature are slightly less (anti)correlated.

C. MRJ Sphere Packings

The pair-correlation function $g_2(r)$ and the correlation functions of the Minkowski functionals of the MRJ sphere packings are shown in Fig. 6. The diameter of the spheres in the MRJ sphere packings is $D \approx 1.07\lambda$. The most striking differences in the pair correlation of the jammed packings to the equilibrium packings are the two discontinuities at $r = \sqrt{3}D$ and $r = 2D$, the split-second peak, which corresponds to configurations of two edge-sharing equilateral and coplanar triangles ($r = \sqrt{3}D$) or a linear chain of three particles ($r = 2D$), respectively [78]. There

is also a significant (seemingly nonanalytic) feature of the volume-volume correlation function $C_{00}(r)$ at $r = \sqrt{3}D$: a dip in the anticorrelation. However, at $r = 2D$, the feature is statistically insignificant. At least two double anticorrelation peaks are clearly resolved.

The most important qualitative differences in the volume-volume correlation function are the much stronger anticorrelations in the MRJ packings compared to the equilibrium packings. The correlation with the nearest neighbors is weaker and the first anticorrelation double peak is more than twice as strong as for the equilibrium hard-sphere packings. The MRJ sphere packings are hyperuniform [29, 45], i.e., large-scale density fluctuations are suppressed. Therefore, strong Voronoi volume anticorrelations are necessary such that Voronoi cells with a high local packing fraction are accompanied by cells with rather low packing fractions, and vice versa.

Another difference between MRJ and equilibrium packings is a stronger shift of the correlation functions of the other Minkowski functionals. For the MRJ packings, there are radial distances, e.g., $r = 2.51\lambda$, at which the integrated mean curvatures are anti-correlated [$C_{22}(2.51\lambda) < 0$] but the volumes are correlated [$C_{00}(2.51\lambda) > 0$], and vice versa.

So, in contrast to the local Voronoi analysis, the global Voronoi analysis of the MRJ packing reveals qualitative structural differences to the equilibrium hard-sphere liquid.

V. CELL-CELL PROBABILITY DENSITY FUNCTIONS

The sampling of the cell-cell probability density function $p(r, v, v^*)$ is very similar to that of the pair-correlation function g_2 (see, e.g., Ref. [4]); only an additional binning with respect to the Voronoi volumes is needed. Figures 7–9 show the cell-cell pair-correlation function $g_{vv} = p(r, v, v^*)/(\rho^2 f(v)f(v^*))$ for exemplary large or small cell volumes v, v^* in the three-dimensional Poisson point process, in an ensemble of equilibrium hard spheres, or in the MRJ sphere packings. As examples of large or small cells, the volumes were chosen such that their probability density is equal to 1/3 of the maximum of the volume distribution; see Table I and Fig. 2.

For the Poisson point process, the small cells are strongly correlated at short distances because, by construction, there must be points at close distances, and the neighbor cells of a small Voronoi cell are more likely to be small as well. However, the probability of finding a point with either a corresponding large or a small cell at a short radial distance of the center of a large cell is strongly suppressed because it is unlikely for the center of a large cell to have close neighbors. At intermediate distances, two large cells are correlated, as expected, because of the Voronoi construction.

In the equilibrium hard-sphere liquid, the large cells at near contact are less correlated than the small cells.

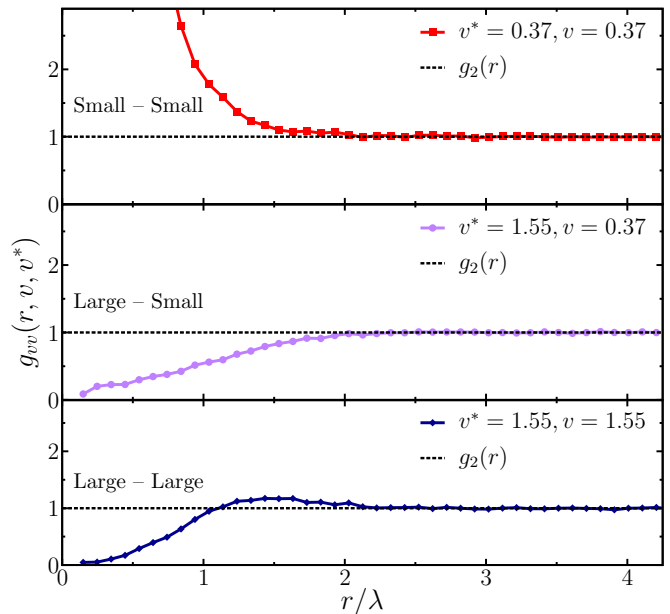


FIG. 7. (Color online) The cell-cell pair-correlation function $g_{vv}(r, v, v^*)$ for a three-dimensional *Poisson point process* for either two large cells (bottom), a large and a small cell (center), or two small cells (top). As examples of large or small cells, the volumes were chosen such that their probability density is equal to 1/3 of the maximum of the volume distribution; see Table I and Fig. 2. The curves are compared to the standard pair-correlation function $g_2(r)$ (dashed black line), which is trivially unity for the uncorrelated Poisson point process. The radial distance r is normalized by $\lambda = 1/\rho^{1/3}$, where ρ is the number density.

However, at slightly larger distances, where g_2 shows anticorrelation and the small cells are even more strongly anti-correlated, the large cells are positively correlated. For distances larger than twice the diameter, the cell-cell pair-correlation function for a large and a small cell is equal to the standard pair-correlation function within statistical significance. However, both the cell-cell pair-correlation functions of finding two short or of finding two large cells at large radial distance r are shifted compared to the standard pair-correlation function.

These features can also be found in the MRJ sphere packings. Moreover, the anticorrelations of two small cells are much stronger. The split-second peak even separates in two stronger peaks with anticorrelation in between, where the standard pair-correlation function shows positive correlation. In contrast to this, the peak at $r = \sqrt{3}D$ completely vanishes for two large cells $g_{vv}(\sqrt{3}D, 1.06, 1.06) = 1$, and the peak at $r = 2D$ is significantly weaker.

VI. CONCLUSIONS AND DISCUSSIONS

We have characterized the structure of MRJ sphere packings by computing the Minkowski functionals, i.e.,

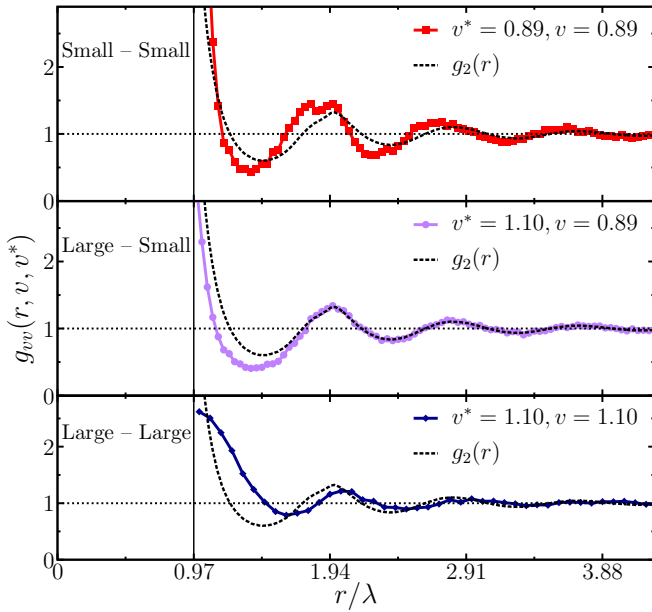


FIG. 8. (Color online) The cell-cell pair-correlation function $g_{vv}(r, v, v^*)$ for *equilibrium hard spheres* at a global packing fraction $\phi = 0.48$; for details, see Fig. 7.

the volume, the surface area, and the integrated mean curvature, of the associated Voronoi cells. The local analysis, i.e., the probability distribution of the Minkowski functionals of a single Voronoi cell, provides qualitatively similar results for the equilibrium hard-sphere liquid and the MRJ packings and partly even for the uncorrelated Poisson point process.

In order to study the global structure of the Voronoi cells, we have improved upon this analysis by introducing the correlation functions $C_{\mu\mu}(r)$ of the Minkowski functionals and the cell-cell probability density function $p(r, v, v^*)$. The correlation function $C_{\mu\mu}(r)$ measures the correlation of the Minkowski functionals W_μ of two Voronoi cells given that the corresponding centers are at a distance r . The cell-cell probability density function $p(r, v, v^*)$ also incorporates the probability that there are two particles at a distance r . For an easier interpretation and better visualization, we have defined the dimensionless cell-cell pair-correlation function $g_{vv} = p(r, v, v^*) / (\rho^2 f(v) f(v^*))$, where $f(v)$ is the probability of the Voronoi volume v . The generalization of the pair-correlation to the cell-cell pair correlations provides powerful theoretical and computational tools to characterize the complex local geometries that arise in jammed disordered sphere packings.

Because the faces of a Voronoi cell are bisections between a point in the point process (whether a packing or not) and its neighbors and, moreover, because Voronoi neighbors share a face and edges, the Minkowski functionals of neighboring Voronoi cells are correlated by construction. This leads to a large correlation length for the Voronoi cells in a Poisson point process because of large Voronoi volume fluctuations. In the equilib-

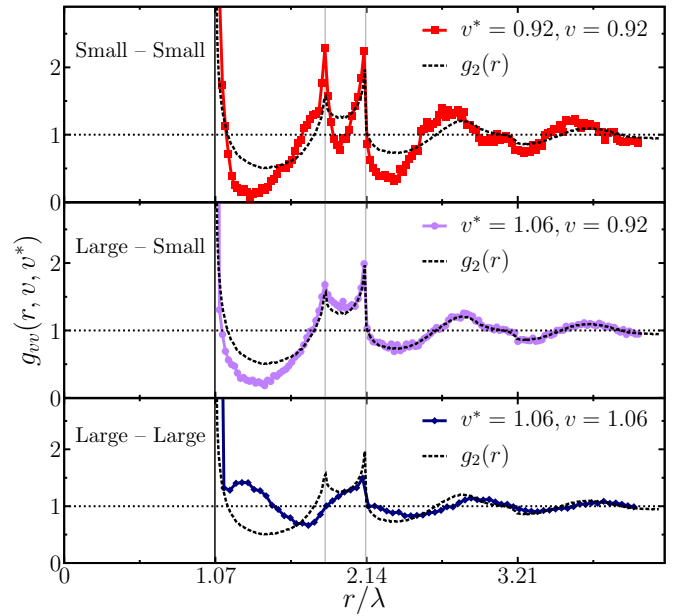


FIG. 9. (Color online) The cell-cell pair-correlation function $g_{vv}(r, v, v^*)$ of the *MRJ sphere packings*; the average packing fraction is $\phi \approx 0.64$; for details, see Fig. 7.

rium hard-sphere liquid and MRJ sphere packings, there are correlations and anticorrelations. In contrast to the qualitatively similar local Voronoi structure, the global Voronoi structure of the MRJ hard-sphere packings is qualitatively quite different from that of an equilibrium hard-sphere liquid. We find strong Voronoi volume anticorrelations, which is consistent with previous findings that MRJ sphere packings are hyperuniform [29, 45], i.e., large-scale density fluctuations are suppressed. MRJ sphere packings are prototypical glasses in that they have no long-range order but they are perfectly rigid, i.e., the elastic moduli are unbounded [19, 37, 79]. The global analysis introduced here shows the difference in the structure of the Voronoi cells of the MRJ state and those of a hard-sphere liquid, which further indicates that the structure of a glass is not that of a “frozen liquid” [45, 79, 80].

An already known distinct structural difference between the hyperuniform MRJ sphere packings and equilibrium hard-sphere liquids is that while in the equilibrium packing the total pair-correlation function $h(r) = g_2(r) - 1$ is exponentially damped, the total correlation function of the MRJ state has a negative algebraic power-law tail [29, 45, 79]. It is an interesting question as to whether the asymptotic behaviors of the correlation function of the Minkowski functionals $C_{\mu\mu}(r)$ or the radial cell-cell correlation functions $g_{vv}(r, v, v^*)$ are different for the MRJ state and the hard-sphere liquid. However, a direct observation of the power-law tail has, so far, not been possible [29, 45, 79]; much larger systems are needed but are not available at the moment. Still, the global characteristics $C_{\mu\mu}(r)$ and $g_{vv}(r, v, v^*)$, introduced in the present paper, allow for an investigation of the underlying

geometrical reasons for the negative algebraic tail in the total pair-correlation function: the suppressed clustering of regions with low and high local packing fractions [45].

Moreover, they also allow for a quantification of the global structure of other cellular structures, e.g., foams, where the centers of mass of the single cells can be used as centers of the cells instead of the Voronoi centers used here.

A frequently discussed question is whether or not there are local icosahedral configurations in jammed packings [14, 20, 21, 31, 81], i.e., a central sphere with 12 spheres in contact where the centers of the touching spheres form a regular icosahedron. The Voronoi cell of the central sphere in such an icosahedron is a regular dodecahedron, which has the maximum possible local packing fraction (≈ 0.76). There is growing evidence, that there are no regular icosahedral arrangements in hard-sphere packings, e.g., see Refs. [14, 78, 82]. Indeed, we find in our MRJ sphere packings no regular and hardly any nearly regular dodecahedral Voronoi cells. All spheres out of more than two million have less than 12 contacts. There are local packing fractions up to 0.75, but only 4.2×10^{-5} of all cells have a local packing fraction greater than 0.74.

In a preliminary approach to look for possibly strongly distorted dodecahedral Voronoi cells in the MRJ sphere packings, we examined the topology of the Voronoi polyhedra, i.e., the number of faces and the corresponding types of polygons, following Refs. [81, 83, 84]. In a compact notation, the topology of a polyhedron is given by the so-called p vector $(n_3 \ n_4 \ n_5 \ n_6)$, where n_3 is the number of triangles, n_4 of quadrilaterals, n_5 of pentagons, and n_6 of hexagons. The dodecahedron is formed by 12 pentagons, i.e., its topology is denoted by $(0 \ 0 \ 12 \ 0)$. Although these polyhedron characteristics are discontinuous and inadequately metric for definite conclusions [85], they can provide a first insight into whether there could be a significant number of distorted dodecahedra. In the MRJ sphere packings, 1.1 % of all cells have the topology of a dodecahedron $(0 \ 0 \ 12 \ 0)$ [86]. The average local packing fraction of those distorted dodecahedra is 0.69 and is thus significantly greater than the total mean local packing fraction which is 0.64. However, only 0.4 % of the distorted dodecahedra have a local packing fraction greater than 0.74. The distorted dodecahedra also have a higher average number of contacts, ≈ 7 , compared to the typical cell, ≈ 6 , but as stated above there is not a single sphere with 12 contacts in this high-quality MRJ data. There are 25 other topologies in the Voronoi diagram of the MRJ sphere packings that occur more frequently than the dodecahedron. With 5.2 % of all cells, the most likely topology is $(0 \ 3 \ 6 \ 5)$. However, by adding one or two faces, the dodecahedron can transform to the following polyhedra [81]: 1.1 % of all cells in the MRJ sphere packings are $(1 \ 0 \ 9 \ 3)$, 3.1 % are $(0 \ 1 \ 10 \ 2)$, and 4.4 % are $(0 \ 2 \ 8 \ 4)$. The latter is the second most common type in the MRJ sphere packings. So, while we find no regular icosahedral configurations in the MRJ sphere packings,

the preliminary topological analysis indicates that more detailed studies of probably strongly distorted icosahedra could be interesting. For example, also in metallic glasses, significant numbers of distorted icosahedra have been found [87, 88].

In the second paper of this series, we will further investigate the global structure of the MRJ sphere packings by looking at density fluctuations, the pore-size distribution, and the two-point correlation functions.

ACKNOWLEDGMENTS

M.K. thanks Klaus Mecke for continuous support and guidance and valuable discussions and advice. We thank Steven Atkinson, Sebastian Kapfer, Adil Mughal, and Gerd Schröder-Turk for valuable discussions and suggestions. This work was supported in part by the National Science Foundation under Grants No. DMR-0820341 and No. DMS-1211087. We also thank the German Science Foundation (DFG) for Grants No. ME1361/11 “Random Fields” and ME1361/12 “Tensor Valuations” awarded as part of the DFG-Forschergruppe “Geometry and Physics of Spatial Random Systems.”

Appendix A: Correlation Functions of the Voronoi cells in the One-Dimensional Poisson Point Process

As an introductory example of the global Voronoi statistics introduced in this paper, we analytically calculate the correlation functions of the Voronoi cells in the one-dimensional Poisson point process. Therefore, we use the probability density functions $H_p(n_l)$ and $H_p(n_r)$ of the nearest neighbor on the left-hand side at a distance n_l or on the right-hand side at a distance n_r , respectively.

Two points x_1 and x_2 at a distance r are given. Without loss of generality, we assume in the following $x_1 = 0$ and $x_2 = r$. The nearest-neighbor probability density functions of x_1 are $H_p(n_l) = \rho e^{-\rho n_l}$ and $H_p(n_r) = \rho e^{-\rho n_r} \theta(r - n_r) + e^{-\rho r} \delta(r - n_r)$, where $\theta(x)$ is the Heaviside step function and $\delta(x)$ is the Dirac delta distribution. For x_2 , the distributions for the right- and the left-hand side simply exchange. The probability distribution $f(v^*|r)$ of the volume v^* of the cell corresponding to $x_1 = 0$ is given by the average of $\delta(\frac{n_r + n_l}{2} - v^*)$:

$$f(v^*|r) = \begin{cases} 4v^*\rho^2 e^{-2v^*\rho} & \text{if } v^* < \frac{r}{2} \\ 2\rho(r\rho + 1)e^{-2v^*\rho} & \text{if } v^* \geq \frac{r}{2} \end{cases} \quad (\text{A1})$$

Given a volume v^* of the cell corresponding to x_1 : If $v^* < r/2$, there will be at least one additional point y between x_1 and x_2 . Its distance z to x_2 is uniformly distributed between $r - 2v^*$ and r . With $h(z|r, v^*)$ denoting the probability density function of this distance, the conditional probability distribution of the volume v of the

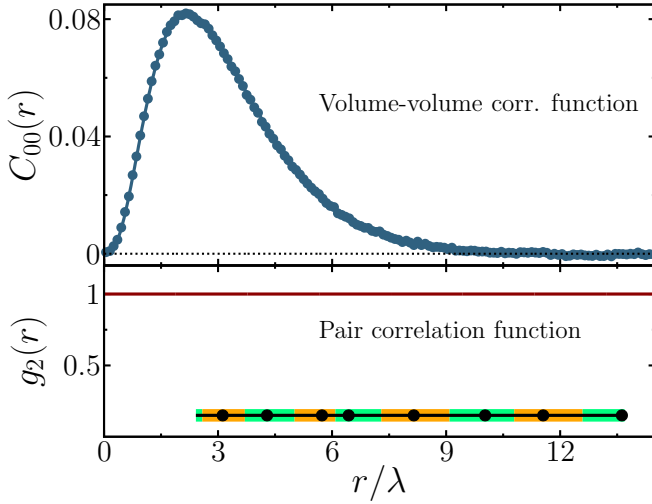


FIG. 10. (Color online) Correlation functions for the one-dimensional Poisson point process: pair-correlation function $g_2(r)$ (bottom); volume-volume correlation function $C_{00}(r)$ (top). The distance r is scaled (in this one-dimensional example) by the inverse of the number density $\lambda = 1/\rho$. An example of a one-dimensional Voronoi diagram of a Poisson point process is depicted.

cell corresponding to x_2 is given by

$$f(v|r, v^*) = \int_0^r dz h(z|r, v^*) \cdot f(v|z) \quad (\text{A2})$$

with $f(v|z)$ from Eq. (A1). A case-by-case analysis for differently large v compared to r and v^* is needed. If $v < \frac{r}{2} - v^*$:

$$f(v|r, v^*) = 4v\rho^2 e^{-2v\rho}. \quad (\text{A3})$$

If $\frac{r}{2} - v^* < v < \frac{r}{2}$, then

$$f(v|r, v^*) = \frac{\rho e^{-2v\rho}}{2v^*} [4v(r-v)\rho - (r-2v^*)^2\rho + 4(v+v^*) - 2r]. \quad (\text{A4})$$

If $v > \frac{r}{2}$, then

$$f(v|r, v^*) = 2\rho e^{-2v\rho} [1 + \rho(r-v^*)]. \quad (\text{A5})$$

If $v^* > r/2$, there will be at least one additional point y between x_1 and x_2 with probability $r\rho/(r\rho+1)$ and with probability $1/(r\rho+1)$ the points x_1 and x_2 are nearest

neighbors. In the first case, the conditional probability distribution of the volume v is given by Eq. (A2), but the distance z is now uniformly distributed between 0 and r . If $v < \frac{r}{2}$, then

$$f(v|r, v^*) = \frac{4v\rho e^{-2v\rho}}{r} ((r-v)\rho + 1). \quad (\text{A6})$$

If $v > \frac{r}{2}$, then

$$f(v|r, v^*) = \rho e^{-2v\rho} (r\rho + 2). \quad (\text{A7})$$

In the second case, where there is no point between x_1 and x_2 , the volume v is at least $r/2$ and completely determined by the nearest neighbor of x_2 on the right-hand side,

$$f(v|r, v^*) = 2\rho e^{r\rho} e^{-2v\rho}. \quad (\text{A8})$$

The cell-cell probability density function $p(r, v, v^*)$ from Sec. III B is then given by

$$p(r, v, v^*) = \rho^2 \cdot f(v^*|r) \cdot f(v|r, v^*). \quad (\text{A9})$$

From Eqs. (A1) and (A3) follows the asymptotic behavior of $p(r, v, v^*) \xrightarrow{r \rightarrow \infty} \rho^2 f(v) f(v^*)$.

As described in Sec. III B, the volume-volume correlation function C_{00} from Sec. III A follows straightforwardly,

$$C_{00}(r) := \frac{r^2 \rho^2 - 2r\rho + 2 - 2e^{-r\rho}}{4 - 4r\rho e^{-r\rho} - 2e^{-2r\rho}} \cdot e^{-r\rho}. \quad (\text{A10})$$

Figure 10 depicts the volume-volume correlation function $C_{00}(r)$ of the one-dimensional Poisson point process; both the analytic result and simulation data are shown.

As discussed in Sec. IV A for the three-dimensional Poisson point process, the Voronoi neighbors are correlated by construction. Although very large Voronoi cells are rather unlikely, their next-neighbor correlation leads to a large correlation length in $C_{00}(r)$. In contrast to the three-dimensional case, the Voronoi neighbors are uncorrelated if the distance of their centers vanishes because in one dimension these Voronoi cells become independent. They only depend on either the nearest neighbor on the left- or on the right-hand side of $x_1 = x_2$, which are independent of each other. For large radii, the correlation vanishes exponentially, as expected, because there is no long-range order in the Voronoi diagram.

-
- [1] P. Chaikin and T. Lubensky, *Principles of Condensed Matter Physics* (Cambridge University Press, Cambridge, 2000).
 - [2] V. N. Manoharan, M. T. Elsesser, and D. J. Pine, *Science* **301**, 483 (2003).
 - [3] J. Hansen and I. McDonald, *Theory of Simple Liquids*

(Elsevier Science, 2006).

- [4] S. Torquato, *Random Heterogeneous Materials: Microstructure and Macroscopic Properties*, Interdisciplinary Applied Mathematics (Springer, Berlin, 2002).
- [5] A. M. Kraynik, D. A. Reinelt, and F. van Swol, *Phys. Rev. E* **67**, 031403 (2003).

- [6] T. Zohdi, *Mech. Mater.* **38**, 969 (2006).
- [7] A. Mejdoubi and C. Brosseau, *J. Appl. Phys.* **101**, 084109 (2007).
- [8] M. Sahimi, *Flow and Transport in Porous Media and Fractured Rock: From Classical Methods to Modern Approaches* (Wiley, New York, 2011).
- [9] J. L. Gevertz and S. Torquato, *PLoS Comput. Biol.* **4**, e1000152 (2008).
- [10] A. Gillman, K. Matouš, and S. Atkinson, *Phys. Rev. E* **87**, 022208 (2013).
- [11] C. L. Henley, *Phys. Rev. B* **34**, 797 (1986).
- [12] C. S. O'Hern, A. J. Liu, and S. R. Nagel, *Phys. Rev. Lett.* **93**, 165702 (2004).
- [13] T. C. Hales, *Ann. Math.* **162**, 1065 (2005).
- [14] T. Aste, M. Saadatfar, and T. J. Senden, *Phys. Rev. E* **71**, 061302 (2005).
- [15] T. Aste and T. Di Matteo, *Phys. Rev. E* **77**, 021309 (2008).
- [16] S. Torquato and F. H. Stillinger, *J. Appl. Phys.* **102**, 093511 (2007).
- [17] J. L. Finney, *Nature (London)* **266**, 309 (1977).
- [18] R. Zallen, *The Physics of Amorphous Solids* (Wiley Interscience, New York, 1998).
- [19] S. Torquato and F. H. Stillinger, *Rev. Mod. Phys.* **82**, 2633 (2010).
- [20] S. C. Kapfer, W. Mickel, K. Mecke, and G. E. Schröder-Turk, *Phys. Rev. E* **85**, 030301 (2012).
- [21] A. S. Clarke and H. Jónsson, *Phys. Rev. E* **47**, 3975 (1993).
- [22] G. T. Seidler, G. Martinez, L. H. Seeley, K. H. Kim, E. A. Behne, S. Zaraneek, B. D. Chapman, S. M. Heald, and D. L. Brewe, *Phys. Rev. E* **62**, 8175 (2000).
- [23] E. R. Weeks and D. A. Weitz, *Phys. Rev. Lett.* **89**, 095704 (2002).
- [24] S. Torquato and F. H. Stillinger, *Exp. Math.* **15**, 307 (2006).
- [25] S. Torquato and Y. Jiao, *Phys. Rev. E* **82**, 061302 (2010).
- [26] G. W. Delaney, T. Di Matteo, and T. Aste, *Soft Matter* **6**, 2992 (2010).
- [27] Y. Jiao, F. H. Stillinger, and S. Torquato, *J. Appl. Phys.* **109**, 013508 (2011).
- [28] M. Palombo, A. Gabrielli, V. D. P. Servedio, G. Ruocco, and S. Capuani, *Sci. Rep.* **3**, 2631 (2013).
- [29] A. Donev, F. H. Stillinger, and S. Torquato, *Phys. Rev. Lett.* **95**, 090604 (2005).
- [30] L. E. Silbert and M. Silbert, *Phys. Rev. E* **80**, 041304 (2009).
- [31] R. Kurita and E. R. Weeks, *Phys. Rev. E* **82**, 011403 (2010).
- [32] L. Berthier, P. Chaudhuri, C. Coulais, O. Dauchot, and P. Sollich, *Phys. Rev. Lett.* **106**, 120601 (2011).
- [33] S. Torquato, T. M. Truskett, and P. G. Debenedetti, *Phys. Rev. Lett.* **84**, 2064 (2000).
- [34] A. R. Kansal, S. Torquato, and F. H. Stillinger, *Phys. Rev. E* **66**, 041109 (2002).
- [35] Note that there are many other more ordered packings with the same packing fraction.
- [36] S. Torquato and F. H. Stillinger, *J. Phys. Chem. B* **105**, 11849 (2001).
- [37] S. Torquato, A. Donev, and F. Stillinger, *Int. J. Solids Struct.* **40**, 7143 (2003).
- [38] The jamming category of a finite system will depend on the boundary conditions; see Refs. [36] and [37].
- [39] S. Atkinson, F. H. Stillinger, and S. Torquato, *Phys. Rev. E* **88**, 062208 (2013).
- [40] E. Marcotte and S. Torquato, *Phys. Rev. E* **87**, 063303 (2013).
- [41] A. Donev, R. Connelly, F. H. Stillinger, and S. Torquato, *Phys. Rev. E* **75**, 051304 (2007).
- [42] B. D. Lubachevsky and F. H. Stillinger, *J. Stat. Phys.* **60**, 561 (1990).
- [43] S. Torquato and F. H. Stillinger, *Phys. Rev. E* **68**, 041113 (2003).
- [44] This determines the asymptotic behavior of the total correlation function and the number variance or density fluctuations within a spherical observation window as a function of the radius of an observation window [29].
- [45] A. B. Hopkins, F. H. Stillinger, and S. Torquato, *Phys. Rev. E* **86**, 021505 (2012).
- [46] J. L. Finney, *P. R. Soc. A Math. Phys.* **319**, 479 (1970).
- [47] F. W. Starr, S. Sastry, J. F. Douglas, and S. C. Glotzer, *Phys. Rev. Lett.* **89**, 125501 (2002).
- [48] F. Lechenault, F. da Cruz, O. Dauchot, and E. Bertin, *J. Stat. Mech.* **2006**, P07009 (2006).
- [49] T. Aste and T. Di Matteo, *Eur. Phys. J. E* **22**, 235 (2007).
- [50] G. E. Schröder-Turk, W. Mickel, M. Schröter, G. W. Delaney, M. Saadatfar, T. J. Senden, K. Mecke, and T. Aste, *Europhys. Lett.* **90**, 34001 (2010).
- [51] S. C. Kapfer, W. Mickel, F. M. Schaller, M. Spanner, C. Goll, T. Nogawa, N. Ito, K. Mecke, and G. E. Schröder-Turk, *J. Stat. Mech. Theory E* **2010**, P11010 (2010).
- [52] S.-C. Zhao, S. Sidle, H. L. Swinney, and M. Schröter, *Europhys. Lett.* **97**, 34004 (2012).
- [53] For each sphere, a Voronoi cell is assigned which contains all points closer to this sphere than to any other sphere in the packing.
- [54] R. Schneider and W. Weil, *Stochastic and Integral Geometry (Probability and Its Applications)* (Springer, Berlin, 2008).
- [55] K. Mecke, *Int. J. Mod. Phys. B* **12**, 861 (1998).
- [56] K. Mecke and D. Stoyan, *Statistical Physics and Spatial Statistics - The Art of Analyzing and Modeling Spatial Structures and Pattern Formation*, 1st ed., Lecture Notes in Physics, Vol. 554 (Springer, Berlin, 2000).
- [57] G. E. Schröder-Turk *et al.*, *Adv. Mater.* **23**, 2535 (2011).
- [58] The Euler characteristic, another Minkowski functional, is a topological constant. For a single Voronoi cell, it is always trivially equal to one.
- [59] G. E. Schröder-Turk, S. C. Kapfer, B. Breidenbach, C. Beisbart, and K. Mecke, *J. Microsc.* **238**, 57 (2010).
- [60] K. Mecke, *Phys. Rev. E* **53**, 4794 (1996).
- [61] J. Becker, G. Grun, R. Seemann, H. Mantz, K. Jacobs, K. R. Mecke, and R. Blossey, *Nat. Mater.* **2**, 59 (2003).
- [62] H. Mantz, K. Jacobs, and K. Mecke, *J. Stat. Mech.* **12**, P12015 (2008).
- [63] C. H. Rycroft, G. S. Grest, J. W. Landry, and M. Z. Bazant, *Phys. Rev. E* **74**, 021306 (2006).
- [64] C. H. Rycroft, *Chaos* **19**, 041111 (2009).
- [65] W. Mickel, S. Münster, L. M. Jawerth, D. A. Vader, D. A. Weitz, A. P. Sheppard, K. Mecke, B. Fabry, and G. E. Schröder-Turk, *Biophys. J.* **95**, 6072 (2008).
- [66] G. E. Schröder-Turk, W. Mickel, S. C. Kapfer, F. M. Schaller, B. Breidenbach, D. Hug, and K. Mecke, *New J. Phys.* **15**, 083028 (2013).
- [67] Because the packing fraction of the equilibrium hard-sphere liquid is lower than for the MRJ state, the corresponding diameters of the spheres are different in this

paper.

- [68] S. Chiu, D. Stoyan, W. Kendall, and J. Mecke, *Stochastic Geometry and Its Applications* (Wiley, New York, 2013).
- [69] The local packing fraction is the volume of the sphere divided by the volume of the Voronoi cell.
- [70] E. Pineda, P. Bruna, and D. Crespo, *Phys. Rev. E* **70**, 066119 (2004).
- [71] The volume distributions are well approximated by shifted γ distributions,

$$f(v) = \frac{1}{\Gamma(k)\theta^k} (v - v_{\min})^{k-1} e^{-(v-v_{\min})/\theta}$$

where the parameters $k = (\langle v \rangle - v_{\min})^2 / \sigma_v^2$ and $\theta = \sigma_v^2 / (\langle v \rangle - v_{\min})$ are determined by the mean $\langle v \rangle$ and standard deviation σ_v of the volume distribution [15]. The volume of a Voronoi cell of a hard-sphere packing must be greater than the volume v_{\min} of a dodecahedron with the sphere touching all of its faces [15, 89].

- [72] The parameters k of the γ distributions are $k = 5.6$ for the Poisson point process, $k = 24.3$ for the equilibrium hard-sphere liquid, and $k = 13.3$ for the MRJ sphere packings.
- [73] The generalized γ distribution is

$$\gamma_q(x) := \frac{q(x - x_{\min})^{q(k-1)} e^{-((x-x_{\min})/\theta)^q}}{\Gamma(k-1+1/q)\theta^{1+q(k-1)}}$$

where the parameter θ is fixed by the mean of the surface area or of the integrated mean curvature; the parameters k and q are fit parameters. The minimum surface area and integrated mean curvature is assumed to be that of a dodecahedron. Note that Lazar *et al.* [74] showed with very high statistics, using 250 000 000 cells, that the Voronoi volume distribution of a Poisson point process also deviates statistically significantly from a two-parameter γ distribution, but is very well described by the generalized γ distribution.

- [74] E. A. Lazar, J. K. Mason, R. D. MacPherson, and D. J. Srolovitz, *Phys. Rev. E* **88**, 063309 (2013).

- [75] The reduced χ squared of the fits to the surface area distributions and integrated mean curvature distributions are for the equilibrium hard-sphere packings 0.94 or 0.96, respectively, and for the Poisson point process 2.40 or 2.43, respectively, but for the MRJ sphere packings, they are 23.2 or 25.7, respectively.
- [76] J. Illian, P. Penttinen, H. Stoyan, and D. Stoyan, *Statistical Analysis and Modelling of Spatial Point Patterns*, Statistics in Practice (Wiley, 2008).
- [77] The distance of two particles is their minimum image separation distance if periodic boundary conditions are applied.
- [78] A. Donev, S. Torquato, and F. H. Stillinger, *Phys. Rev. E* **71**, 011105 (2005).
- [79] É. Marcotte, F. H. Stillinger, and S. Torquato, *J. Chem. Phys.* **138**, 12A508 (2013).
- [80] T. M. Truskett, S. Torquato, and P. G. Debenedetti, *Phys. Rev. E* **62**, 993 (2000).
- [81] J. Finney, *Mater. Sci. Eng.* **23**, 199 (1976).
- [82] S. C. Kapfer, Ph.D. thesis, Friedrich-Alexander-Universität Erlangen-Nürnberg, 2011.
- [83] D. Barnette, *J. Comb. Theory* **7**, 99 (1969).
- [84] E. A. Lazar, J. K. Mason, R. D. MacPherson, and D. J. Srolovitz, *Phys. Rev. Lett.* **109**, 095505 (2012).
- [85] J. Finney and J. Wallace, *J. Non-Cryst. Solids* **43**, 165 (1981).
- [86] In the equilibrium hard-sphere liquid, 0.45 % of all cells are distorted dodecahedra; in a Poisson Voronoi tessellation, the fraction is less than 2×10^{-5} .
- [87] G. W. Lee, A. K. Gangopadhyay, K. F. Kelton, R. W. Hyers, T. J. Rathz, J. R. Rogers, and D. S. Robinson, *Phys. Rev. Lett.* **93**, 037802 (2004).
- [88] A. Hirata, L. J. Kang, T. Fujita, B. Klumov, K. Matsue, M. Kotani, A. R. Yavari, and M. W. Chen, *Science* **341**, 376 (2013).
- [89] S. Torquato and Y. Jiao, *Phys. Rev. E* **87**, 022111 (2013).